

**Area-selective atomic layer deposition of noble metals
Polymerized fluorocarbon layers as effective growth inhibitors**

Deminskyi, Petro; Haider, Ali; Eren, Hamit; Khan, Talha M.; Biyikli, Necmi

DOI

[10.1116/6.0000701](https://doi.org/10.1116/6.0000701)

Publication date

2021

Document Version

Accepted author manuscript

Published in

Journal of Vacuum Science and Technology A: Vacuum, Surfaces and Films

Citation (APA)

Deminskyi, P., Haider, A., Eren, H., Khan, T. M., & Biyikli, N. (2021). Area-selective atomic layer deposition of noble metals: Polymerized fluorocarbon layers as effective growth inhibitors. *Journal of Vacuum Science and Technology A: Vacuum, Surfaces and Films*, 39(2). <https://doi.org/10.1116/6.0000701>

Important note

To cite this publication, please use the final published version (if applicable).
Please check the document version above.

Copyright

Other than for strictly personal use, it is not permitted to download, forward or distribute the text or part of it, without the consent of the author(s) and/or copyright holder(s), unless the work is under an open content license such as Creative Commons.

Takedown policy

Please contact us and provide details if you believe this document breaches copyrights.
We will remove access to the work immediately and investigate your claim.

Area-selective atomic layer deposition of noble metals: polymerized fluorocarbon layers as effective growth inhibitors

Running title: Selective metal deposition via polymerized CF_x inhibition layers

Running Authors: Deminskyi *et al.*

Petro Deminskyi,¹ Ali Haider,¹ Hamit Eren,² Talha M. Khan,¹ Necmi Biyikli^{3,a)}

¹UNAM-Institute of Materials Science and Nanotechnology, Bilkent University, Ankara 06800, Turkey

²Department of Chemical Engineering, Delft University of Technology, van der Maasweg 9, 2629 HZ Delft, The Netherlands

³Electrical and Computer Engineering, University of Connecticut, 371 Fairfield Way, Storrs, CT, 06269-4157

a) Electronic mail: necmi.biyikli@uconn.edu

The increasingly complex nanoscale three-dimensional (3D) and multi-layered structures utilized in nanoelectronic, catalytic, and energy conversion/storage devices, necessitate novel substrate-selective material deposition approaches featuring bottom-up and self-aligned precision processing. Here, we demonstrate the area-selective atomic layer deposition (AS-ALD) of two noble metals, Pt and Pd, by using plasma polymerized fluorocarbon layer as growth inhibition surfaces. Contact angle, X-ray photoelectron spectroscopy (XPS), and scanning electron microscopy (SEM) measurements were performed to investigate the blocking ability of polymerized fluorocarbon (CF_x) layers against ALD-grown metal films. Both Pt and Pd showed significant nucleation delays on fluorocarbon surfaces. Self-aligned film deposition is confirmed using this strategy by growing Pt and Pd on microscale lithographically patterned CF_x/Si samples. CF_x blocking layer degradation during ozone exposure was analyzed using XPS measurements which confirmed the oxygen physisorption as the main responsible surface reaction with further

hydroxyl group formation on CF_x surface. Our work reveals that CF_x layer is compatible with ozone co-reactant until the blocking polymer cannot withstand oxygen physisorption. Our results could potentially be used to investigate and develop radical-assisted AS-ALD processes for a wider selection of materials.

I. INTRODUCTION

Atomic-scale precision manufacturing of next-generation complex three-dimensional (3D) device structures necessitates the development of highly-selective bottom-up material deposition strategies. As opposed to the conventional top-down approaches, area-selective deposition (ASD) provides self-aligned processing capability, which enhances the structural precision while reducing the overall fabrication complexity. The relatively recent efforts in area-selective atomic layer deposition (AS-ALD) unveiled the significant potential of ALD as a bottom-up materials synthesis technique which can be engineered towards achieving surface selectivity.¹⁻⁵ Being a surface-chemistry driven vapor-phase synthesis method, ALD features iterative self-limiting growth cycles based on low-temperature ligand-exchange reactions.^{6,7} The resulting deposition is highly controllable with sub-monolayer thickness accuracy, along with excellent 3D conformity and large-area uniformity.⁸⁻¹⁴ The main target of AS-ALD efforts is to combine the unique features of ALD with surface selectivity, potentially leading to a versatile self-aligned fabrication tool-box.

Among others, area-deactivation approach became the main AS-ALD strategy, where self-assembled monolayers (SAMs) or various polymer films are utilized as growth blocking surfaces.^{15,16} This way, selective deposition has been reported for oxides,^{4,17-19} (Al_2O_3 , SiO_2 , TiO_2 , ZnO) and metals²⁰⁻²³ (Pt, Pd, Ru, Rh, Ir, Co). Despite the

promising results with various SAM chemistries, this approach suffered mainly from the difficulty in defect-free SAM synthesis, relatively long synthesis time, and CMOS-compatibility.^{4,24-26} The latest reports by Bent et al. show that the time for SAM deposition reduced significantly with vapor-phase techniques instead of conventional liquid-phase synthesis, and yet provides sufficient blocking performance for conventional thermal AS-ALD processes.^{1,27} However, both SAM and polymer blocking layers tend to degrade fairly quickly when radical-enhanced co-reactants are utilized including plasmas and ozone. This incompatibility with energetic co-reactants limits their use to merely thermal-ALD processes which excludes some critical materials.^{28,29}

Platinum (Pt) and palladium (Pd) are amongst the most widely employed noble metals not only for CMOS logic and memory device fabrication,^{30,31} but as well for catalysis,³² energy conversion,³³ chemical sensing,^{34,35} and energy storage.³⁶ Selective deposition of these noble metals is significantly needed for the fabrication of self-aligned metal-contact placement in 3D nanoscale device structures. Reports on AS-ALD of Pd are mostly related to the controlled synthesis of Pd/Pt core-shell nanoparticles using SAMs as blocking layers.³⁷ On the other hand, former efforts related to the AS-ALD of Pt include (i) electron-beam induced deposition,³⁸ which has compatibility issues for large areas and high-aspect-ratio structures, (ii) use of PMMA and polyimide (PI) blocking layers for thermal Pt-ALD which degrade under radical/plasma exposure,³⁹ and (iii) topographically selective Pt-ALD on the vertical sidewalls of fin structures via ion-implanted ultrathin fluorocarbon films as growth inhibition horizontal surfaces.² Selective noble-metal ALD featuring energetic co-reactants such as ozone are yet missing. Growth inhibitors needed for such energetic ALD processes should ideally exhibit sufficient

radical-resistance, a defect/pinhole-free microstructure, CMOS-compatibility, ease of deposition, and thermal stability.¹⁵

Our previous work on AS-ALD of metal-oxide films where we used inductively coupled plasma (ICP)-polymerized fluorocarbon (CF_x) coatings as blocking layers, showed effective ZnO growth inhibition with self-aligned patterning, while no growth blocking efficiency was observed for TiO₂.^{40,41} Utilization of a CMOS-standard plasma-polymerized CF_x film along with its relative ease of control, revealed this approach with significant potential. In this work, we demonstrate that polymerized fluorocarbon surfaces can function as effective growth inhibitors for ALD-grown Pt and Pd films as well. Besides providing successful growth blocking for Pt and Pd, ozone-assisted Pt ALD experiments revealed that polymerized CF_x layers are also ozone-compatible. To the best of our knowledge, this is the first demonstration of an AS-ALD process utilizing ozone as co-reactant for noble metals. When compared to the ion-implanted ultra-thin CF_x blocking layers,² our approach provides a complementary CMOS-compatible solution to inhibit Pt and Pd deposition on non-horizontal surfaces of 3D nanostructures. This strategy might pave the way for the selective deposition of alternative materials which necessitate energetic co-reactants.

II. EXPERIMENTAL

1. *Film growth:*

CF_x layer was deposited in a commercial ICP etch reactor (SPTS MPX-ICP), conventionally used for deep reactive ion etching (DRIE) process of Si wafers. Deposition of ~60 nm of CF_x was performed for ~70 sec using C₄F₈ (99.998 % purity,

Linde) gas flow rate of 70 sccm, under 400 W radio frequency plasma power at 13.56 MHz. Si (100) reference control samples were solvent cleaned (acetone, isopropyl alcohol, de-ionized water rinse, and N₂ blow dry) and exposed to O₂ plasma in an asher system (100 W, 50 sccm) for 2 minutes before ALD of Pd in order to increase the concentration of hydroxyl groups on the substrate which should eliminate any possible nucleation delays on Si surface.⁴⁰ The reference control samples for Pt study were not pre-treated in O₂ plasma before the main Pt ALD growth due to the ozone-based plasma process that increases the hydroxyl groups on the substrate during the deposition experiments. Pt and Pd deposition on bare and CF_x-coated Si (100) samples was accomplished by using trimethyl (methylcyclopentadienyl) platinum(IV) (MeCpPtMe₃) and palladium(II) hexafluoroacetylacetonate (Pd(hfac)₂) as metal precursors.^{42,43} Ozone (O₃) and formalin (CH₂O) were utilized as co-reactants for Pt and Pd growth, respectively.^{44,45} O₃ was produced from a pure O₂ flow with a Veeco/Cambridge NanoTech Savannah Ozone Generator. ALD experiments with different cycle numbers were carried out at 150 and 200 °C for Pt and Pd respectively, using a Savannah S100 ALD reactor, (Veeco/CambridgeNanoTech Inc.) using N₂ as the carrier and purge gas. The unit ALD-growth cycle of Pt consisted of MeCpPtMe₃ pulse (0.2 s), N₂ purge (15 s), ozone pulse (0.1 s), and N₂ purge (15 s). MeCpPtMe₃ precursor was preheated to 65°C and stabilized at this temperature to transport the MeCpPtMe₃ vapor to the reaction chamber. On the other hand, the unit ALD cycle of Pd consisted of Pd(hfac)₂ pulse (0.4 s), N₂ purge (10 s), formalin pulse (0.15 s), and N₂ purge (10 s). Pd(hfac)₂ precursor was preheated to 70 °C and stabilized at this temperature prior to deposition experiments.

Formalin was kept at room temperature during the growth. Total stabilization time before growth both for Pt and Pd was ~20 min.

2. *Film characterization and patterning:*

Contact angle of bare and CF_x-coated Si (100) substrates have been measured before and after ALD growth cycles, using static contact angle measurement setup (OCA 30). A 4 μL-water droplet was dropped on the sample surfaces to measure the contact angle. Film thicknesses of CF_x have been determined using a variable angle spectroscopic ellipsometer (V-VASE, J.A. Woollam Co. Inc., Lincoln, NE) which is coupled with a rotating analyzer and xenon light source. The ellipsometric spectra were collected at three angles of incidence (65°, 70°, and 75°) to yield adequate sensitivity over the full spectral range. Film thickness values were extracted by fitting the spectroscopic ellipsometer data using Cauchy model, while the substrate was set as default Si (100) in V-Vase Woollam software. Elemental composition and chemical bonding states of the metal films were obtained by XPS measurements using Thermo Scientific K-Alpha spectrometer (Thermo Fisher Scientific) with a monochromatized Al K α X-ray source (spot size ~400 μm). All peaks in XPS survey scans are referenced to C 1s peak for charge correction and quantification of survey scans have been performed using Avantage software. Surface morphologies of Pt and Pd-coated samples were determined using high-resolution FIB-SEM system (FEI, Nova 600i Nanolab) and the cluster size were determined using “Image J” software. To pattern CF_x via lithography on Si (100) substrates, ~1.4 μm of AZ5214 photoresist (Microchemicals GmbH) is spun on the wafer and is patterned into a checkerboard and parallel striped lines using a suitable photomask and photolithography. The wafer is then hard baked at 110°C for 5 min, followed by the

ICP-polymerization process in the ICP reactor. Once the deposition is complete, the wafer is soaked into acetone for lift-off process of the CF_x layer portions on top of the patterned photoresist. The resulting wafer with patterned CF_x layer is solvent-cleaned before subsequent metal-ALD growth experiments. XPS line-scan was performed on the resulting Pt and Pd-coated samples to determine the selectivity performance as a function of ALD cycles, using the same XPS system with a spot size of $\sim 100 \mu m$, scanning step size and scanning points of 41/43 μm and 100/176 for Pt/Pd, respectively. Structural analysis of ALD grown Pt and Pd thin films were performed using grazing-incidence X-ray diffraction (GIXRD) patterns that were recorded in an X'Pert PRO MRD diffractometer (PANalytical B.V., Almelo, Netherlands) using $Cu K\alpha$ radiation. Data were obtained within the 2θ range of $30 - 90^\circ$ by the summation of ten scans, which were performed using 0.1° step size and 15 s counting time. Interplanar spacing (d_{hkl}) values were calculated from peak positions using Bragg's law. Lattice parameter was calculated by using the experimentally extracted d_{hkl} values in Equation (1), which relates the interplanar spacing (d_{hkl}), miller indices (hkl), and lattice parameter (a_0) for face-centered cubic (fcc) crystal system.

$$d_{hkl} = \frac{a_0}{\sqrt{h^2+k^2+l^2}} \quad (1)$$

To determine the growth selectivity values for Pt and Pd as a function of ALD cycles, we used Equation (2), which is based on the measured XPS elemental concentrations of Pt or Pd on CF_x (non-growth) and Si (growth) surfaces:

$$Selectivity = \frac{A_{Si} - B_{CFx}}{A_{Si}}, \quad (2)$$

where A_{Si} and B_{CF_x} – are the atomic % of ALD deposited material on Si and CF_x surfaces respectively. The sensitivity of our selectivity numbers are therefore limited by the XPS detection limit, which is typically around or slightly higher than 0.01 at.%.

III. RESULTS AND DISCUSSION

A. *Pt nucleation and selectivity*

A.1. *Pt nucleation: CF_x vs Si (100) surfaces*

In the first part of our selective deposition study, Pt film nucleation and growth behavior on CF_x and Si surfaces via ozone-based low-temperature ALD is explored. Initial contact angles of Si and CF_x/Si samples before the ALD cycles were measured as $\sim 71^\circ$ and $\sim 114^\circ$, respectively. After the initial 50 ALD cycles, the contact angles on the same samples were measured as 77.4° and 106.4° , respectively, marking an increase for Si and decrease for CF_x surfaces. The contact angle on Si (100) decreased to $\sim 67.4^\circ$ after 250 Pt-ALD cycles, while it remained almost unchanged for CF_x coated sample with a relatively narrow fluctuation between $\sim 104^\circ$ and 106° up to 250 cycles (Fig. 1a). Subsequently, we analyzed the evolution of Pt nucleation by measuring the Pt-island/cluster size on Si and CF_x samples as a function of ALD cycles. Figure 1b shows how the average Pt cluster size evolved on both sample surfaces with increasing the number of ALD cycles, which clearly indicates a considerable nucleation delay on CF_x surface. While no Pt clusters were detected up to 150 cycles, ~ 2 nm and ~ 5 nm Pt cluster were observed on CF_x samples after 200 and 250 ALD cycles, respectively, with relatively low density and surface coverage with respect to Si (100) reference samples. On the other hand, Pt nucleated easily on Si (100) surface exhibiting high-density ~ 3 nm

sized Pt clusters after the initial 50 ALD cycles which increased and saturated up to ~15 nm for 200 and higher ALD cycles.

Figure 2(a–e) and 2(f–j) show the obtained images from the Si (100) and CF_x sample surfaces after 50, 100, 150, 200, and 250 ALD cycles, respectively. The initial 50 cycle results clearly reveals successful Pt nucleation on Si (100) with increase in both Pt nanoparticle (NP) density and cluster size leading towards coalescence into larger islands (~15 nm for 200+ cycles) and eventually complete surface coverage resulting in a continuous Pt film. However, in contrast to the bare Si (100) sample, CF_x/Si sample surface is free from any HR-SEM-detectable Pt nucleation at the end of 150 ALD cycles. Pt nucleation on CF_x becomes evident only after 200 ALD cycles with initial average Pt-cluster diameter of ~2 nm and relatively non-uniform surface distribution. As a result, the initial Pt NP seeds on CF_x surface function as growth centers during the further ALD cycles featuring half-cycle exposures of C₉H₁₆Pt and ozone. The average Pt cluster size increases to ~5 nm at 250 cycles which signs the considerable modification of CF_x surface, not being able to block the rapid Pt-nucleation after 200 growth cycles.

Table I summarizes how the platinum and oxygen content from the surface of CF_x/Si and Si (100) samples evolve during ALD cycles via XPS survey scans. Other than Pt and O content – more detailed information related to the elemental composition of Si, C, and F are presented in Table SI, SII. XPS measurements of the CF_x sample surface show the absence of a detectable Pt signal for 50 and 100 ALD cycles. After 150 ALD cycles, a very weak Pt signal is detected, corresponding to only ~0.01 at. %, which increases by almost an order of magnitude – but still relatively low (~0.07 at. %) for 200 ALD cycles. Further increase in Pt-ALD cycles up to 250 cycles indicates a stronger

increase of Pt content to ~2.6 at. %, confirming the practical Pt-nucleation onset for ALD cycles around 200.

The combination of the adsorption of the noble metal precursor and the use of reactive ozone starts to show its effect on ICP-polymerized CF_x surface only after 200 ALD growth cycles. XPS measurements of the CF_x coated sample exposed to 250 Pt-ALD cycles show oxygen content fluctuating within ~2–4 at. %. It confirms the relative stability of ICP-polymerized CF_x surface against degradation during reactive ozone exposure till the formation of hydroxyl groups (that behave like nucleation centers for Pt growth) and subsequently adsorbed Pt on the surface. To the best of our knowledge, this result represents the first demonstration of a selective ALD process featuring reactive ozone coreactant for Pt deposition.

TABLE I. Variation in Pt and O at. % on CF_x/Si samples and selectivity value as a function of ALD cycles.

Number of ALD cycles	on CF_x/Si		Pt/Si to Pt/ CF_x selectivity
	Pt at. %	O at. %	
50	–	1.03	
100	0.01	1.57	~1
150	0.01	1.81	
200	0.1	2.17	~0.99
250	2.62	4.44	~0.95

Figure 3a shows the XPS survey scan results obtained for CF_x/Si samples recorded at 50, 100, 150, 200, and 250 ALD cycles. While detecting C 1s, O 1s, and F 1s peaks from CF_x surface, absence of Pt 4f peak confirms the successful Pt-nucleation inhibition for more than 150 ALD cycles. These results confirm the effective nucleation inhibition

behavior of ICP-polymerized CF_x films as growth blocking surfaces for Pt deposition. Moreover, the XPS survey scan results provide excellent correlation with SEM observations as well as contact angle measurements and cumulatively approve that CF_x inhibits Pt nucleation process for ~ 200 growth cycles, which is equivalent to a growth blocking thickness of ~ 17 nm. The ~ 0.99 selectivity at 200 cycles drops to ~ 0.95 at 250 ALD cycles.

Figure 3b shows the analysis study on the reaction-resistance of the fluorocarbon layer exposed to ozone-based growth reactions via investigating the O 1s peaks on the CF_x/Si substrate before and after 100, 200, and 250 cycles of Pt ALD growth cycles from the measured XPS scans. O 1s is detected on the CF_x substrate before and after Pt growth, with the O 1s peak located at 531.1 eV (I) corresponds to hydroxyl groups (OH) on the surface of CF_x that is in good agreement with hydroxide signal (531.5 ± 0.5 eV) which is a typical value for binding energies for oxides.⁴⁶ We also note another interesting observation: on CF_x surface, the O 1s peak is broadening to the lower binding energies with the peak intensity at 529.7 eV (II) for 250 cycles of Pt ALD, which could be assigned to the oxygen atoms directly bound to metallic Pt.^{47,48} The mechanism of the Pt nucleation on CF_x is currently not fully understood. We hypothesize that during the ozone half-reaction, oxygen is slowly physisorbed onto the CF_x film surface. This diffusion is likely enhanced during additional ozone exposure cycles. In the meantime, during the MeCpPtMe_3 half-reaction, hydroxyl groups form on the centers of oxygen vacancies that create the favorable nucleation centers for further Pt growth initiation. Although the hydroxyl groups are created on CF_x surface, the amount of Pt that could be chemisorbed on such active sites is still under the XPS-detection limit up to 150 ALD cycles.

Figure 4 shows Pt 4f HR-XPS scans measured on CF_x/Si samples. HR-XPS scans taken after 50, 100, 150, 200, and 250 cycles of Pt-ALD. XPS measurements of CF_x coated Si samples after 50, 100, 150, 200, and 250 cycles of Pt-ALD show no considerable Pt signal up to 200 cycles (Fig. 4a and Table SIII). At 200 and 250 cycles, we started to observe signals in the range of 67–79 eV corresponding to Pt 4f peaks. After XPS data fitting, we deconvoluted the Pt 4f peak into two well-separated ($\Delta = \sim 3.3$ eV) spin-orbit components with height ratio 1:0.77 (Fig. 4b,c). For the 200-cycle sample, Pt 4f peaks centered at 70.7 ± 0.2 eV (subpeak A – Pt 4f_{7/2}) and 74.0 ± 0.2 eV (subpeak B – Pt 4f_{5/2}), are assigned to the metallic Pt(0) bonding. Likewise, we deconvoluted Pt 4f peak for the 250-cycle sample into two individual peaks centered at 70.7 ± 0.2 eV (subpeak A – Pt 4f_{7/2}) and 74.0 ± 0.2 eV (subpeak B – Pt 4f_{5/2}), which are assigned to the same metallic Pt. Pt 4f_{7/2} and Pt 4f_{5/2} are not clearly separated from each other, which could be attributed to the platinum oxidation that resulted in the shoulder formation.⁴⁹ Furthermore, the slightly lower binding energies (70.7 ± 0.2 eV) possibly indicates the presence of smaller Pt particles, which is also in a good agreement with the cluster size dependence on the total ALD cycle number (Fig. 1b and Fig. 2d,i and Fig. 2e,j).⁵⁰ Additional information related to the Pt HR-XPS scans measured on Si samples is represented in the supporting document, which is in good agreement with the observed trend on CF_x/Si (100) samples: oxide states within the initial 50–100 cycles were transformed to metallic states at higher ALD cycle numbers. The HR-XPS scans of Pt 4f on Si (100) are provided in Figure S1.

Another important observation was the thickness stability (~ 60 nm) of CF_x blocking layer regardless of the Pt ALD cycles which featured reactive ozone exposures. Absence of any decrease in CF_x thickness under ozone cycles might be attributed to the

relatively strong C-F bonding which prevented any film etching reaction during excessively long ozone exposure at temperatures up to 150°C. In addition to the inherent unreactive nature of CF_x , stability in the thickness of CF_x layers reminds potential for further investigation of AS-ALD under alternative energetic co-reactants and plasma chemistries in radical-assisted ALD processes.

The structural properties of Pt film were studied by GIXRD. Figure 5(a,b) depict the XRD pattern and SEM image of the as-prepared Pt film with ~20 nm thickness. The measured pattern was indexed by face-centered cubic (fcc) crystal system (ICDD reference code: 00-004-0802). The (111), (200), (220), (311), and (222) peaks reflections were observed at the 2θ values of 40.2°, 46.6°, 67.9°, 81.9°, and 86.3°. The XRD peaks of Pt thin film were comparable to those of the corresponding bulk Pt material.⁴⁹ The lattice parameter a was calculated using 2θ positions of the (111) reflection. Interplanar spacing (d_{hkl}) values was calculated from Bragg's law and the a -axis lattice parameter was calculated as ~ 3.88 Å, which matches well with the bulk value for Pt (3.92 Å).

A.2. Selective Pt deposition and self-aligned patterning

Self-aligned patterning of Pt films is demonstrated using selective Pt deposition on lithographically patterned CF_x/Si samples with 180 Pt-ALD cycles and by EDX analysis, XPS line scan measurements, and HR-SEM imaging as shown in Fig. 6(a-c). XPS line scan was performed on mm-scale Pt patterns (Fig. 6a) where Pt 4f intensity was measured (Fig. 6b). Pt 4f peak is only observed in bright-looking regions where CF_x layer was lifted-off with Si (100) growth surface exposed, while CF_x regions with dark color contrast exhibit Pt 4f intensity as background (noise-floor) signal, confirming the absence of Pt deposition on CF_x non-growth surface. The reason of a gradual increase in Pt 4f

intensity at the CF_x/Si (100) boundaries can be attributed to the relatively larger spot size of the monochromatized Al $K\alpha$ X-ray source that was set to $\sim 100\ \mu\text{m}$ during the XPS line-scan, as well as the value of scanning steps and a number of scanning points utilized. At the CF_x/Pt interface, due to the relatively large XPS spot size, we simultaneously detect signals from both CF_x and Pt covered surfaces which causes a gradual increase in the observed Pt intensity. The uniform blocking of Pt growth on the CF_x pattern was confirmed by the HR-SEM image which depicts a sharp CF_x/Pt interface (see Fig. 6a). Figure 6c shows the EDX line-scan measurement, revealing Pt M X-ray quanta being detected along the scan-line. As expected, the intensity of Pt M X-ray quanta increases only in line-patterns where CF_x was lifted-off with exposed Si (100) surface, which reaffirms the effective self-aligned patterning of Pt line structures at the micro-scale.

EDX elemental mapping images are shown in Fig. 7, which are performed to indicate the coverage and distribution of Pt, C, and F elements on the patterned CF_x/Si sample surface. Figure 7a shows the SEM image of patterned Pt line features through which elemental maps of Pt, C, and F are collected. Figure 7(b-d) show elemental maps of C K, Pt M, and F K, respectively. These results confirm both successful self-aligned patterning of CF_x and area-deactivated AS-ALD deposition of Pt up to at least 180 ALD cycles. We have used 180 cycles of Pt-ALD to avoid any Pt nucleation which appeared after 200 growth cycles and to demonstrate optimal conditions for Pt nucleation on Si growth surface while CF_x non-growth surface shows near-ideal nucleation blocking.

B. Pd nucleation and selectivity

B.1. Pd nucleation: CF_x vs Si (100) surfaces

The Pd-ALD growth experiments using Pd(hfac)₂ and formaline precursors were carried out on CF_x-coated and bare Si (100) substrates for 200, 400, 600, 800, 1000, 1500, and 2000 ALD cycles. [Figure 8\(a,b\)](#) depict the variation in the measured contact angle and average Pd-cluster size of the exposed substrates as a function of the number of ALD cycles. At the end of the first 200 Pd-ALD cycles, the contact angle of Si sample decreased from ~71° to ~57°, while CF_x-coated sample exhibited only a slight decrease from ~114° to ~110°. With further increase in ALD-cycles up to 2000 cycles on Si (100) samples, contact angle exhibited an increase and fluctuated between ~68–72°. The increase of the contact angle with increasing of the number of ALD-cycles ([Figure 8a](#)) can be attributed to the topography (the impact of the surface roughness due to the changes in palladium nanoparticles dimensions ([Figure 8b](#))).^{50,51} In contrast, CF_x samples exhibited rather a stable contact angle values around ~109°, almost independent from the number of ALD cycles up to 1000 cycles. However, the contact angle decreased to ~95° for Pd growth cycles higher than 1500, signaling a possible nucleation onset for Pd film growth on CF_x surface. These results indicate that plasma polymerized CF_x layer retains its rather hydrophobic and inert character up to more than 1000 Pd-ALD cycles while its surface state starts to show an initial change towards 1500 ALD cycles.

Subsequently, SEM measurements were performed to visualize the nucleation behavior of Pd on CF_x-coated and bare Si (100) sample surfaces. [Figure 9\(a–e\)](#) and [9\(f–j\)](#) represent HR-SEM images of Pd ALD on bare and CF_x-coated Si (100) samples after 200, 600, 1000, 1500, and 2000 ALD cycles, respectively. In agreement with the contact angle measurements, HR-SEM images apparently show no measurable evidence of Pd growth on CF_x surface up to the maximum 2000 ALD cycles we have studied. This is in

strong contrast to Pd nucleation and growth behavior on Si (100), where Pd nucleates right away and Pd NPs are apparent after the first 200 ALD cycles. Further increase in Pd growth cycles on Si (100) leads to an increase in density and size of Pd-NPs, eventually coalescing into larger and densely packed Pd islands, with an estimated effective film thickness of ~10 nm. On the other hand, polymerized CF_x film retained its growth blocking character till the maximum number (2000) of growth cycles tested. Literature reports indicate that organic blocking layers used for selective ALD, exhibit degradation beyond certain number of ALD growth cycles, eventually resulting in unwanted nucleation and failure to block film growth. This result has in part been attributed to cumulatively long exposures of the organic blocking layers to relatively high substrate temperatures. Although CF_x layer showed significant inhibition against Pd growth up to 2000 ALD cycles (!12 hours exposure at 200 °C), this does not imply that CF_x won't fail eventually. These results are achieved without a detailed and systematic recipe optimization for Pd growth since the main aim of this study was to explore the noble-metal nucleation inhibition properties of the polymerized CF_x layers. As a follow-up study, the ALD growth conditions might be further adjusted to achieve enhanced selectivity performance via shorter unit ALD-cycles.

[Table II](#) summarizes the quantification of Pd content (at. %) from XPS survey scans for Pd on CF_x/Si and bare Si (100) substrates. Other than Pd content – information related to the elemental composition of Si, C, O, F are presented in [Table SIV](#). The amount of Pd on CF_x/Si samples was calculated as ~ 0.02 % using XPS data, regardless of the number of ALD cycles up to 1500 cycles. This result again confirms that CF_x is efficiently blocking Pd nucleation for at least 1500 ALD cycles. With an additional 500

cycles, the 2000-cycle Pd-ALD sample on CF_x/Si substrate indicates a slight but yet observable increase to ~0.12 %. Despite the fact that this atomic percentage corresponds to typically less than a monolayer of Pd deposition, we can safely claim that the complete Pd-nucleation blocking property of ICP-polymerized CF_x is degraded after 2000 cycles of Pd-ALD. Pd content on bare Si (100) substrate samples, on the other hand, show a strongly correlated increase with number of ALD growth cycles, confirming the absence of Pd nucleation inhibition of Si surfaces.

TABLE II. Variation in Pd at. % on CF_x/Si samples and the calculated selectivity value as a function of ALD cycles.

Number of ALD cycles	on CF _x /Si Pd at. %	Pd/Si to Pd/CF _x selectivity
200	0.02	
400	0.03	
600	0.03	~1
800	0.03	
1000	0.02	
1500	0.03	
2000	0.12	~0.99

XPS survey-scan data from both Si and CF_x samples were recorded at various growth stages to determine the surface elemental composition as well as the chemical bonding states (see Fig. 10). C 1s, O 1s, and F 1s peaks were detected from CF_x surface irrespective of the number of Pd-ALD cycles. Absence of as detectable Pd 3d peak corroborate the previous findings that CF_x successfully blocks Pd film growth throughout the entire 2000 ALD cycles (Fig. 10b). On the other hand, on bare Si (100) surface, the presence of relatively strong Pd 3d peak signals right after the very first 200 ALD cycles,

confirms Si (100) surface as an efficient growth surface with no or small nucleation delay (Fig. 10a).

To further analyze and confirm Pd nucleation inhibition on CF_x surface, Pd 3d high-resolution XPS (HR-XPS) scans were carried out and the resulting peak spectra measured on Si (100) and CF_x/Si (100) as a function of total ALD cycles are shown in Fig. 11. All recorded peaks were fitted after a charge-correction with respect to the adventitious C 1s spectra component (C-C, C-H) with binding energy set to 284.8 eV. HR-XPS spectra exhibits Pd 3d_{5/2} and Pd 3d_{3/2} spin-orbit doublet peaks for the ALD-grown Pd on bare Si (100) substrates, which represent the growth surface for our experiments. The detected bonding species, their corresponding spectral lines, and binding energy values for the grown Pd film have been summarized in Table SV. For the initial 200 and 400 growth cycles, Pd-O and Pd-O_x bonding scheme have also been detected in addition to the main Pd-Pd core level bonding. Figure 11a shows that beyond 400 growth cycles, Pd 3d_{5/2} and Pd 3d_{3/2} peaks corresponding only to Pd-Pd bonding interactions have been detected, confirming the formation of small Pd clusters leading to larger Pd agglomerations and eventually Pd thin films with complete surface coverage.^{52,53} On the contrary, no detectable Pd signal is observed in the HR-XPS data obtained from CF_x/Si samples (Fig. 11b) inferring near-ideal Pd-nucleation inhibition on CF_x blocking layers up to 2000 ALD cycles.

Figure 12 displayed the XRD pattern and SEM image of the as-prepared ~15 nm thin film, showing the characteristic of the property of the crystalline Pd. The exhibited pattern was indexed by face-centred cubic (fcc) crystal system (ICDD reference code: 00-046-1043). The (111), (200), (220), (311) and (222) peaks reflections were observed at

the 2θ values of 39.9° , 46.4° , 67.7° , 81.4° , and 86.2° which is in agreement with previously reported results.⁵⁴ The lattice parameter a was similarly calculated using 2θ positions of (111) reflection. The extracted a -axis lattice parameter was 3.91 \AA , which matches well with the bulk lattice parameter value for Pd (3.89 \AA).⁵⁵

B.2. Selective Pd deposition and self-aligned patterning

Similar to our selective Pt deposition study, we carried out self-aligned Pd film patterning experiments via selective Pd deposition on lithographically patterned CF_x/Si substrates. Positive CF_x patterns were formed for the analysis and visualization of possible edge effects in selective Pd-growth on Si (100) and growth inhibition on CF_x , respectively. Pd deposition was carried out for 2000 ALD cycles on patterned CF_x/Si samples which are subsequently characterized by HR-SEM, EDX line scan, EDX elemental mapping, and XPS line scan measurements. [Figure 13\(a,b\)](#) show SEM images of the Pd patterns which legibly indicate the selective deposition of Pd metal (brighter regions) along with clear and uncoated CF_x surface (darker circular spots). HR-SEM image from the Pd/ CF_x interface shows no Pd deposition signs on top of polymerized CF_x patterns except a narrow transition region (50–100 nm) corresponding to the width of the lifted-off CF_x layer sidewall. Within these transition areas, Pd nanoparticles with smaller cluster size and lower density are observed most probably due to the imperfections of the conventional photolithographic patterning process.

To analyze the elemental composition variation along the Pd/ CF_x patterns, EDX and XPS line scan was performed, as depicted in [Fig. 14](#). XPS line scan was performed on larger mm-scale Pd patterns ([Fig. 14a](#)) as the survey spectra for this measurement were recorded with an X-ray beam size of $400 \mu\text{m}$, along with $\sim 50 \mu\text{m}$ steps between

each data point. Pd 3d intensity was measured in terms of counts per second vs. spatial location along the line (Figure 14b). A considerable contrast is observed between the Pd 3d peak signal intensity obtained from the lifted-off Si (100) regions where Pd has grown without a significant nucleation delay and CF_x patterns which blocked Pd nucleation effectively, confirmed with a signal intensity equal to the noise floor of the XPS system. The EDX line-scan (Fig. 14c) reveals that the intensity of Pd L X-ray quanta increases only within the non-CF_x coated line features which reaffirm the successful self-aligned deposition of Pd via polymerized fluorocarbon growth inhibitors.

Figure 15 represents the EDX elemental mapping analyses of Pd, C, and F elements at specific patterned areas after the 2000-cycle ALD experiment. Figure 15a shows the SEM image of the patterned Pd line features through which elemental maps of Pd, C, and F are collected. Figure 15(b-d) depict elemental maps of C K, Pd L, and F K, respectively. It is evident from these elemental maps that Pd is only present in the line features which coincide with the Pd lines covering the non-CF_x coated regions shown in Fig. 15a. Overall, XPS, EDX line scan, and EDX elemental mapping cumulatively confirm the successful self-aligned patterning via selective Pd deposition using 2000-cycle ALD on lithographically patterned samples.

IV. SUMMARY AND CONCLUSIONS

In conclusion, we have presented a systematic investigation on the growth blocking/inhibition efficacy of plasma-polymerized CF_x layers to achieve selective deposition of Pt and Pd. We have demonstrated an effective yet relatively simple approach for low-temperature self-aligned patterning of Pt and Pd films using a CMOS-

compatible plasma-polymerization process. The recorded nucleation delays for Pt and Pd correspond to equivalent blocking thicknesses of ~20 nm and ~15 nm, respectively, with selectivity values of ~0.99 for both Pt and Pd deposition. This work confirms that plasma-polymerized CF_x layers effectively inhibit film growth not only for certain oxide compounds, but as well for widely used noble metals (Pt, Pd). The reason for CF_x blocking layer degradation during the ozone-based ALD process was concluded to be due to the oxygen physisorption with further hydroxyl groups formation on CF_x surface that creates the favorable nucleation sites for Pt growth initiation. Our methodology can be utilized for various 3D device structures where selective Pt/Pd deposition on horizontal surfaces might be critically needed while blocking on other inclined and vertical surfaces via conformally coated CF_x blocking layers. Moreover, the ozone-compatible selective deposition capability might pave the way for the AS-ALD of a wider set of materials which can benefit from ozone and alternative energetic co-reactants.

ACKNOWLEDGMENTS

The authors acknowledge (1) Institute of materials science and nanotechnology (UNAM), Bilkent University for the growth and material characterization facilities; (2) TUBITAK for their support under 2216 project for International Researcher; (3) University of Connecticut – Research Excellence Program (REP) Grant funded by the Office of the Vice President for Research (OVPR).

SUPPORTING INFORMATION

This material is available online free of charge and includes the following documents:

XPS survey scan; high-resolution XPS scans; variation in C, F at. % on CF_x/Si and C, Si at. % as a function of Pt ALD cycles; Pt binding energies on Si and on CF_x/Si; variation in C, F, O at. % on CF_x/Si and C, Si at. % on Si as a function of Pd ALD cycles; Pd binding energies.

The data that support the findings of this study are available from the corresponding author upon reasonable request.

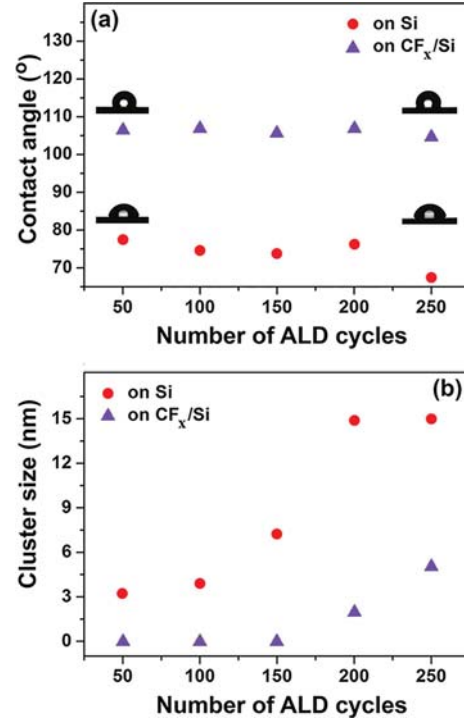
- ¹S. F. Bent (*ASD-2017*, 20–21 April, Eindhoven, The Netherlands, 2017).
- ²W.-H. Kim, F. S. M. Hashemi, A. J. M. Mackus, J. Singh, Y. Kin, D. Bobb-Semple, Y. Fan, T. Kaufman-Osborn, L. Godet, S. F. Bent, et al., *ACS Nano* **10**, 4451 (2016).
- ³J. Singh, N. F. W. Thissen, N. F.W. Thissen, W. H. Kim, H. Johnson, W. M. M. Kessels, A. Bol, S. F. Bent, A. J. M. Mackus, *Chem. Mater.* **30**, 663 (2018).
- ⁴E. Färm, M. Kemell, M. Ritala, M. Leskelä, *Thin Solid Films*, **517**, 972 (2008).
- ⁵E. Stevens, Y. Tomczak, B. T. Chan, E. A. Sanchez, G. N. Parsons, A. Delabie, *Chem. Mater.*, **30**, 10, 3223 (2018).
- ⁶S. M. George, *Chem. Rev.*, **110**, 111 (2010).
- ⁷M. Leskela, M. Ritala, *Thin Solid Films*, **409**, 138 (2002).
- ⁸C. J. Serpell, J. Cookson, D. Ozkaya, P. D. Beer, *Nat. Chem.*, **3**, 478 (2011).
- ⁹A. J. M. Mackus, D. Garcia-Alonso, H. C.M. Knoops, A. A. Bol, W. M. M. Kessels, et al. *Chem. Mater.*, **25**, 1769 (2013).
- ¹⁰J. Hämäläinen, F. Munnik, M. Ritala, M. Leskelä, *Chem. Mater.*, **20**, 6840 (2008).
- ¹¹M. Knez, K. Nielsch, L. Niinisto, *Adv. Mater.*, **19**, 3425 (2007).
- ¹²M. D. Groner, F. H. Fabreguette, J. W. Elam, S. M. George, *Chem. Mater.*, **16**, 639 (2004).

- ¹³B. S. Lim, A. Rahtu, R. G. Gordon, *Nat. Mater.*, **2**, 749 (2003).
- ¹⁴J. Tang, Q. Cao, G. Tulevski, K. A. Jenkins, L. Nela, D. B. Farmer, S.-J. G. Han, *Nat. Electron.*, **1**, 191 (2018).
- ¹⁵A. J. M. Mackus, A. A. Bol, W. M. M. Kessels, *Nanoscale*, **6**, 10941 (2014).
- ¹⁶K. Cao, J. Cai, X. Liu, R. Chen, *J. Vac. Sci. Technol. A*, **36**, 010801 (2018)
- ¹⁷S. Seo, B. C. Yeo, S. S. Han, C. M. Yoon, J. Y. Yang, J. Yoon, C. Yoo, H.-J. Kim, Y.-B. Lee, S. J. Lee, J.-M. Myoung, H.-B.-R. Lee, W.-H. Kim, I.-K. Oh, H. Kim, *ACS Appl. Mater. Interfaces*, **9**, 41607 (2017).
- ¹⁸A. Marnett, M. J. M. Merckx, B. Karasulu, F. Roozenboom, W. M. M. Kessels, A. J. M. Mackus, et al. *ACS Nano*, **11**, 9303 (2017).
- ¹⁹C. R. Ellinger, S. F. Nelson, *Chem. Mater.*, **26**, 1514 (2014).
- ²⁰M. Junige, M. Löffler, M. Geidel, M. Albert, J. W. Bartha, E. Zschech, B. Rellinghaus, and W. F. van Dorp, *Nanotechnol.*, **28**, 395301 (2017).
- ²¹K. J. Park, G. N. Parsons, *Appl. Phys. Lett.*, **89**, 043111 (2006).
- ²²X. R. Jiang, H. Huang, F. B. Prinz, S. Bent, *Chem. Mater.*, **20**, 3897 (2008).
- ²³A. J. M. Mackus, S. A. F. Dielissen, J. J. L. Mulders, W. M. M. Kessels, *Nanoscale*, **4**, 4477 (2012).
- ²⁴J. Hong, D. W. Porter, R. Sreenivasan, P. C. McIntyre, S. Bent, *Langmuir*, **23**, 1160 (2007).
- ²⁵M. H. Park, Y. J. Jang, H. M. Sung-Suh, M. M. Sung, *Langmuir*, **20**, 2257 (2004).
- ²⁶J. R. Avila, E. J. Demarco, J. D. Emery, O. K. Farha, M. J. Pellin, J. T. Hupp, A. B. F. Martinson, *ACS Appl. Mater. Interfaces*, **6**, 11891 (2014).
- ²⁷F. Sadat, M. Hashemi, B. R. Birchansky, S. F. Bent, *ACS Appl. Mater. Interfaces*, **8**, 33264 (2016).
- ²⁸J.-Y. Kim, D.-S. Kil, J.-H. Kim, S.-H. Kwon, J.-H. Ahn, J.-S. Roh, S.-K. Park, *Electrochem. Soc.*, **159**, H560 (2012).

- ²⁹J. Hämäläinen, M. Ritala, M. Leskelä, *Chem. Mater.*, **26**, 786 (2014).
- ³⁰Z. Chen, J. Appenzeller, J. Knoch, Y. Lin, P. Avouris, *Nano Lett.*, **5**, 1497 (2005).
- ³¹A. Javey, J. Guo, Q. Wang M. Lundstrom, H. Dai, *Nature*, **424**, 654 (2003).
- ³²X. Luo, M. Piernavieja-Hermida, J. Lu, T. Wu, J. Wen, Y. Ren, D. Miller, Z. Z. Fang, Y. Lei, K. K. Amine, *Nanotechnology*, **26**, 164003 (2015).
- ³³Y. Jiang, J. Chen, J. Zhang, A. Li, Y. Zeng, F. Zhou, G. Wang, and R. Wang, *RSC Adv.*, **6**, 13207 (2016).
- ³⁴D. Gu, H. Baumgart, K. Tapily, P. Shrestha, G. Namkoong, X. Ao, F. Müller, *Nano Res.*, **4**, 164 (2011).
- ³⁵K. Kim, H. B. R. Lee, R. W. Johnson, J. Tanskanen, N. Liu, M. G. Kim, C. Pang, C. Ahn, F. S. Bent, Z. Bao, *Nat. Commun.*, **5**, 4781 (2014).
- ³⁶S. Fleischmann, A. Tolosa, M. Zeiger, B. Krüner, N. J. Peter, I. Grobelsek, A. Quade, A. Kruth, V. Presser, *J. Mater. Chem. A*, **5**, 2792 (2017).
- ³⁷K. Cao, Q. Zhu, B. Shan, R. Chen, *Sci. Rep.*, **5**, 8470 (2015).
- ³⁸A. J. M. Mackus, J. J. L. Mulders, M. C. M. Sanden, W. M. M. Kessels, *J. Appl. Phys.*, **107**, 116102 (2010).
- ³⁹R. H. J. Vervuurt, A. Sharma, Y. Jiao, W. M. M. Kessels, A. Bol, *Nanotechnol.*, **27**, 405302 (2016).
- ⁴⁰A. Haider, P. Deminskyi, T. M. Khan, H. Eren, N. Biyikli *J. Phys. Chem. C*, **120**, 26393 (2016).
- ⁴¹A. Haider, M. Yilmaz, P. Deminskyi, H. Eren, N. Biyikli, *RSC Adv.*, **6**, 106109 (2016).
- ⁴²T. Aaltonen, M. Ritala, Y.-L. Tung, Y. Chi, K. Arstila, K. Meinander, and M. Leskelä, *J. Mater. Res.*, **19** (11), 3353-3358 (2004).
- ⁴³J. J. Senkevich, G.-R. Yang, T.-M. Lu, T. S. Cale, C. Jezewski, W. A. Lanford *Chem. Vap. Deposition*, **8**, 189 (2002).

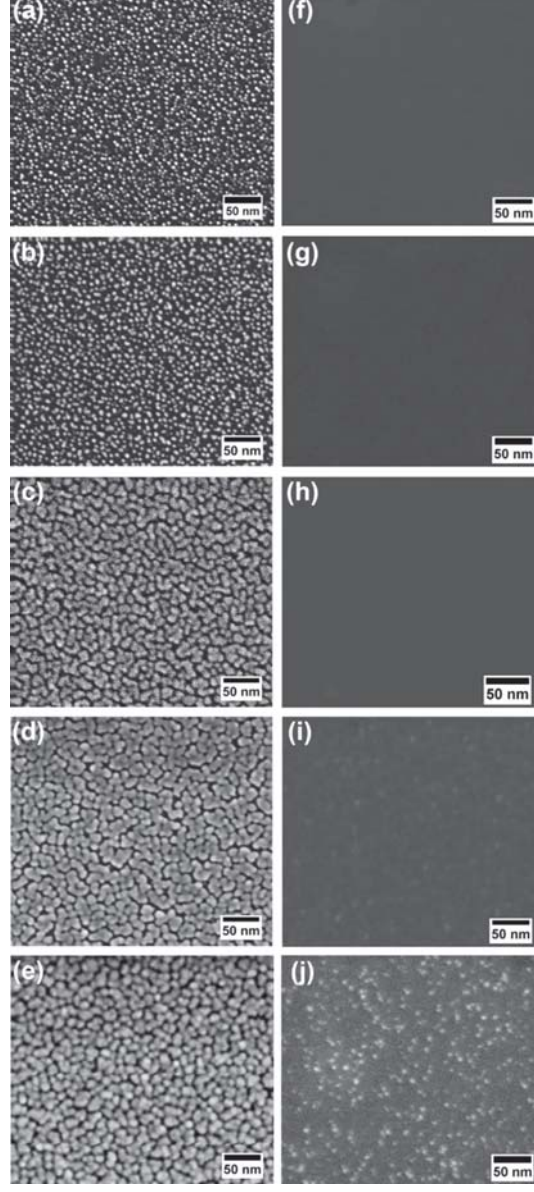
- ⁴⁴J. Dendooven, R. K. Ramachandran, K. Devloo-Casier, G. Rampelberg, M. Filez, H. Poelman, G. B. Marin, E. Fonda, and C. Detavernier, *J. Phys. Chem. C*, **117** (40), 20557–20561 (2013).
- ⁴⁵J.W. Elam, A. Zinovev, C.Y. Han, H.H. Wang, U. Welp, J.N. Hryn, M.J. Pellin, *Thin Solid Films*, **515**, 1664–1673 (2006).
- ⁴⁶M. Peukert *Electrochimica Acta.*, **29**(10), 1315 (1984).
- ⁴⁷T. Nakamura, S. Ichihara, T. Den, *ECS Transactions*, **3**(25), 275 (2007).
- ⁴⁸M. Wakisaka, H. Suzuki, S. Mitsui, H. Uchida, M. Watanabe, *J. Phys. Chem. C*, **112**(7), 2750 (2008).
- ⁴⁹T. Ioroi, K. J. Yasuda, *Electrochem. Soc.*, **152**(10), A1917 (2005).
- ⁵⁰B. Bhushan, Y. C. Jung, *Ultramicroscopy*, **107**, 1033 (2007).
- ⁵¹S. Hoshian, V. Jokinen, V. Somerkivi, A. R. Lokanathan, and S. Franssila, *ACS Appl. Mater. Interfaces*, **7**, 941 (2015).
- ⁵²K. L. Kelly, E. Coronado, L. L. Zhao, G. C. Schatz, *J. Phys. Chem. B*, **107**, 668 (2003).
- ⁵³D. Astruc, *Nanoparticles and Catalysis*. (Wiley-VCH: New York, 2008).
- ⁵⁴L. Xu, X.-C. Wu, J.-J. Zhu, *Nanotechnol.*, **19**(305603), 6 (2008).
- ⁵⁵C. Kittel, *Einführung in die Festkörperphysik*, R. Oldenbourg Verlag Munchen Wien, (John Wiley&Sons GmbH Frankfurt am Main, 1973), 128.

This is the author's peer reviewed, accepted manuscript. However, the online version of record will be different from this version once it has been copyedited and typeset.
PLEASE CITE THIS ARTICLE AS DOI: 10.1116/6.0000701



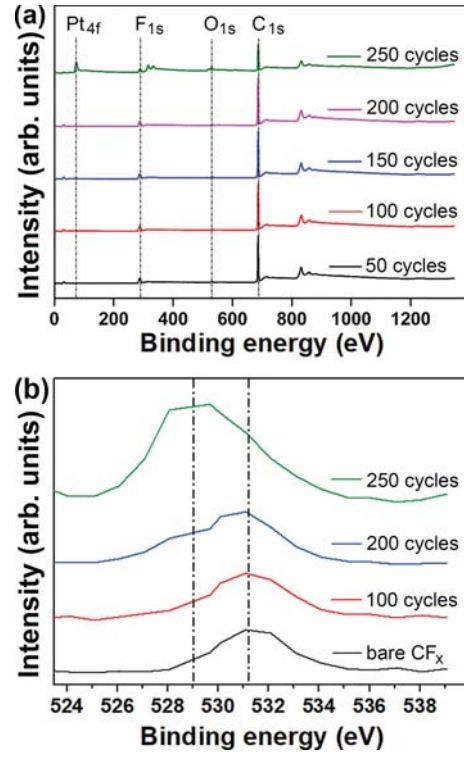
This is the author's peer reviewed, accepted manuscript. However, the online version of record will be different from this version once it has been copyedited and typeset.

PLEASE CITE THIS ARTICLE AS DOI: 10.1116/6.0000701

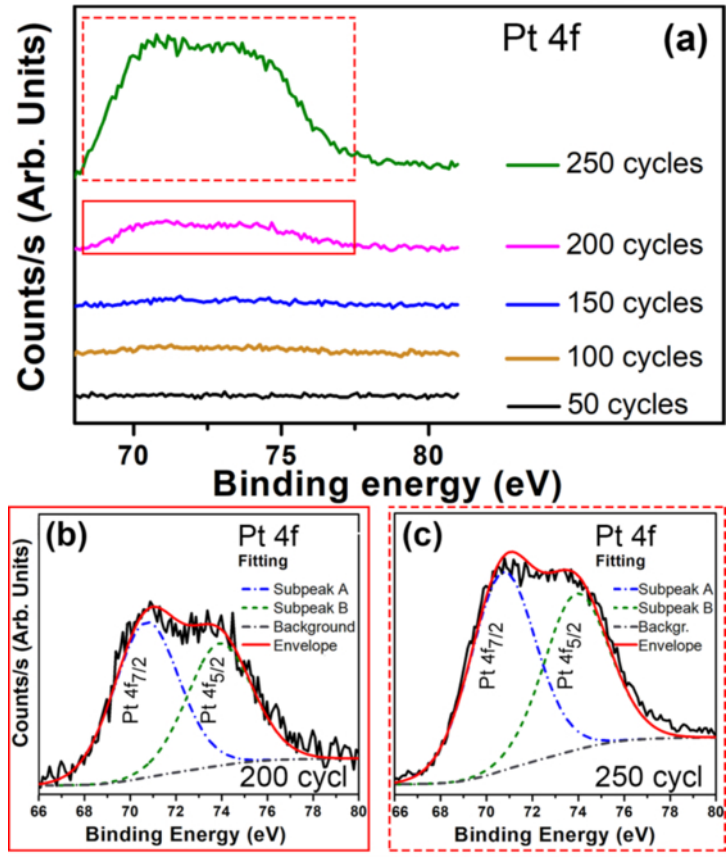


This is the author's peer reviewed, accepted manuscript. However, the online version of record will be different from this version once it has been copyedited and typeset.

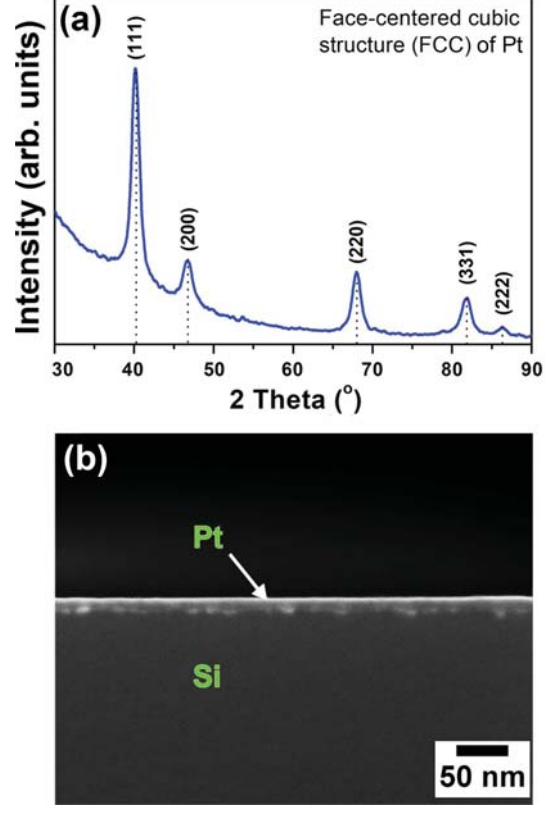
PLEASE CITE THIS ARTICLE AS DOI: 10.1116/6.0000701



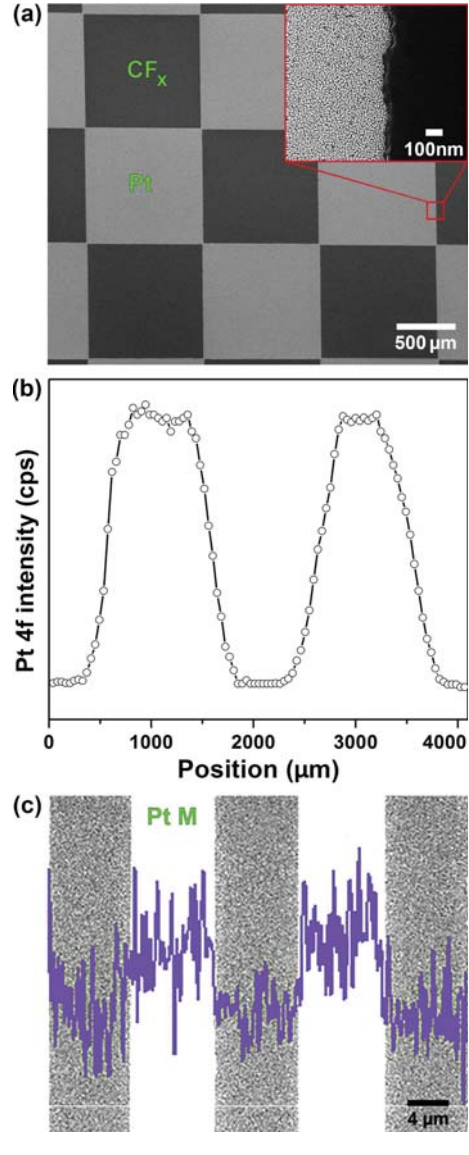
This is the author's peer reviewed, accepted manuscript. However, the online version of record will be different from this version once it has been copyedited and typeset.
PLEASE CITE THIS ARTICLE AS DOI: 10.1116/6.0000701



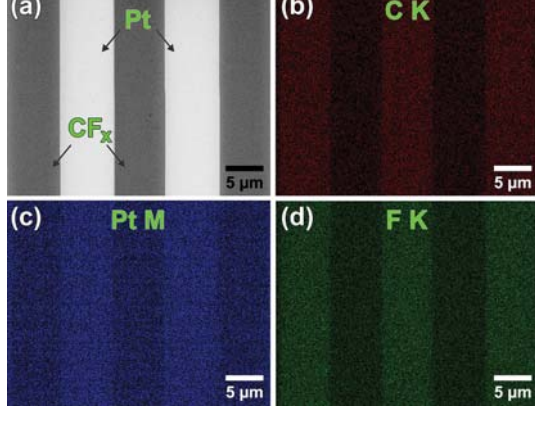
This is the author's peer reviewed, accepted manuscript. However, the online version of record will be different from this version once it has been copyedited and typeset.
PLEASE CITE THIS ARTICLE AS DOI: 10.1116/6.0000701



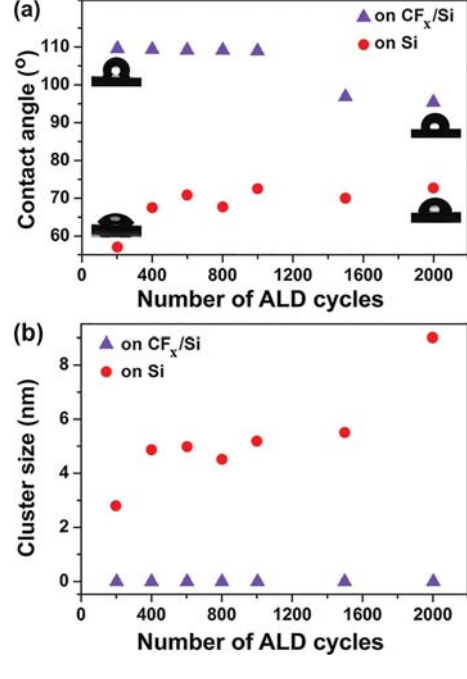
This is the author's peer reviewed, accepted manuscript. However, the online version of record will be different from this version once it has been copyedited and typeset.
PLEASE CITE THIS ARTICLE AS DOI: 10.1116/6.0000701



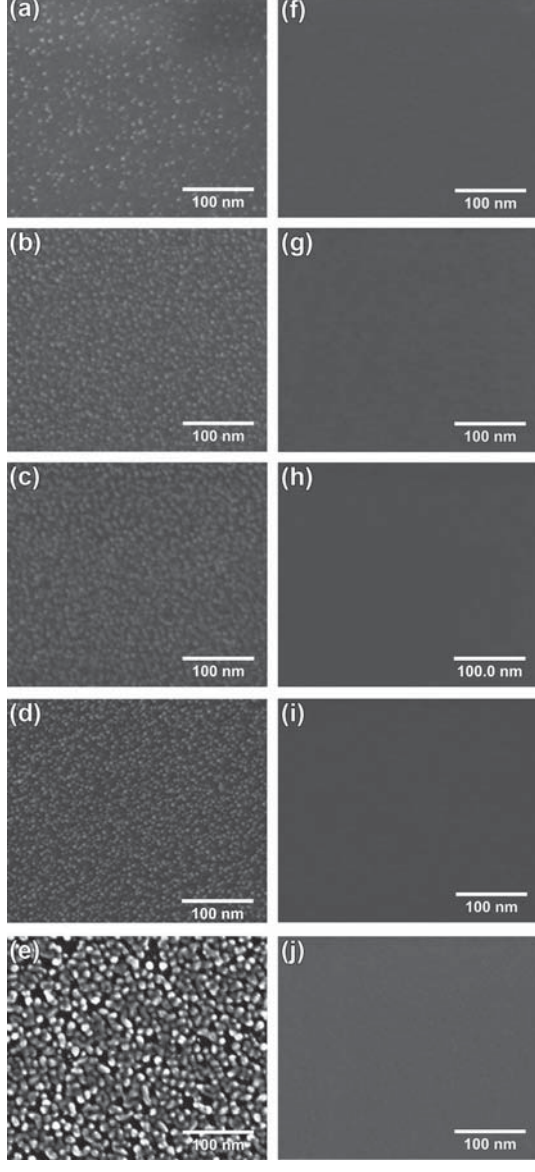
This is the author's peer reviewed, accepted manuscript. However, the online version of record will be different from this version once it has been copyedited and typeset.
PLEASE CITE THIS ARTICLE AS DOI: 10.1116/6.0000701



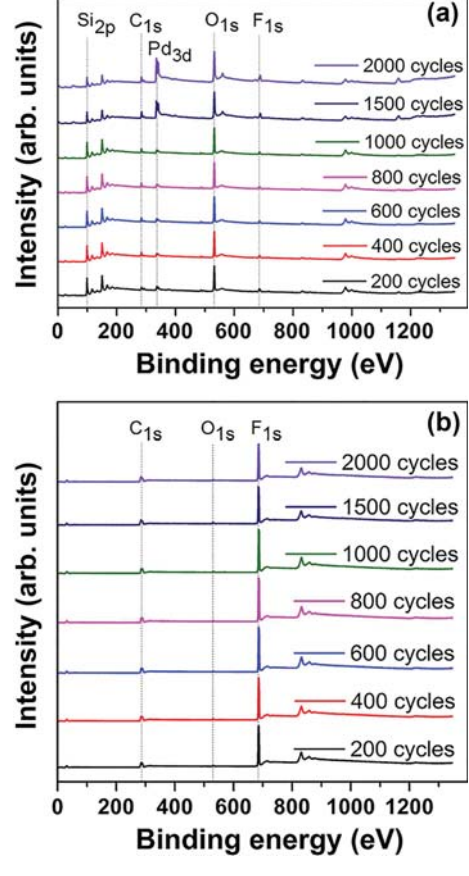
This is the author's peer reviewed, accepted manuscript. However, the online version of record will be different from this version once it has been copyedited and typeset.
PLEASE CITE THIS ARTICLE AS DOI: 10.1116/6.0000701



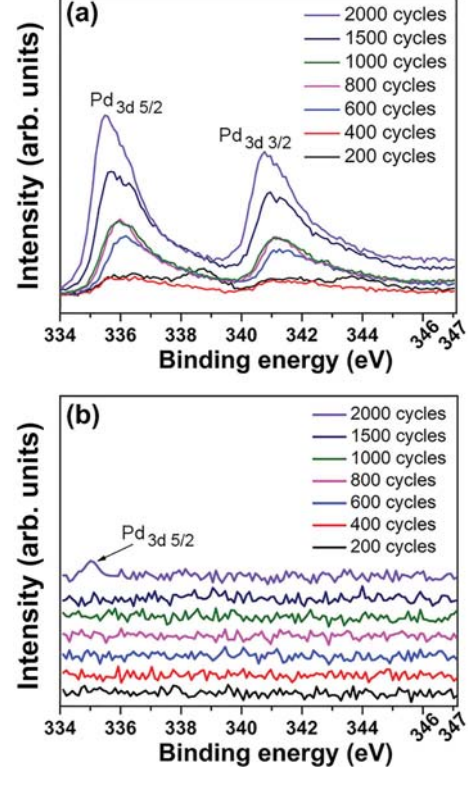
This is the author's peer reviewed, accepted manuscript. However, the online version of record will be different from this version once it has been copyedited and typeset.
PLEASE CITE THIS ARTICLE AS DOI: 10.1116/6.0000701



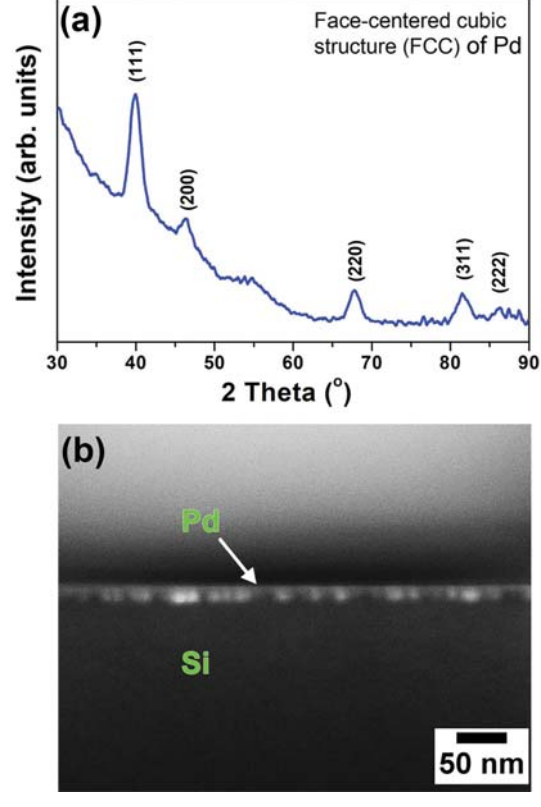
This is the author's peer reviewed, accepted manuscript. However, the online version of record will be different from this version once it has been copyedited and typeset.
PLEASE CITE THIS ARTICLE AS DOI: 10.1116/1.6.0000701



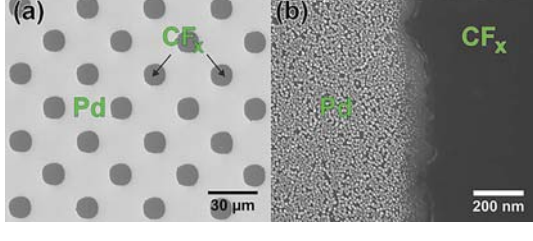
This is the author's peer reviewed, accepted manuscript. However, the online version of record will be different from this version once it has been copyedited and typeset.
PLEASE CITE THIS ARTICLE AS DOI: 10.1116/1.6.0000701



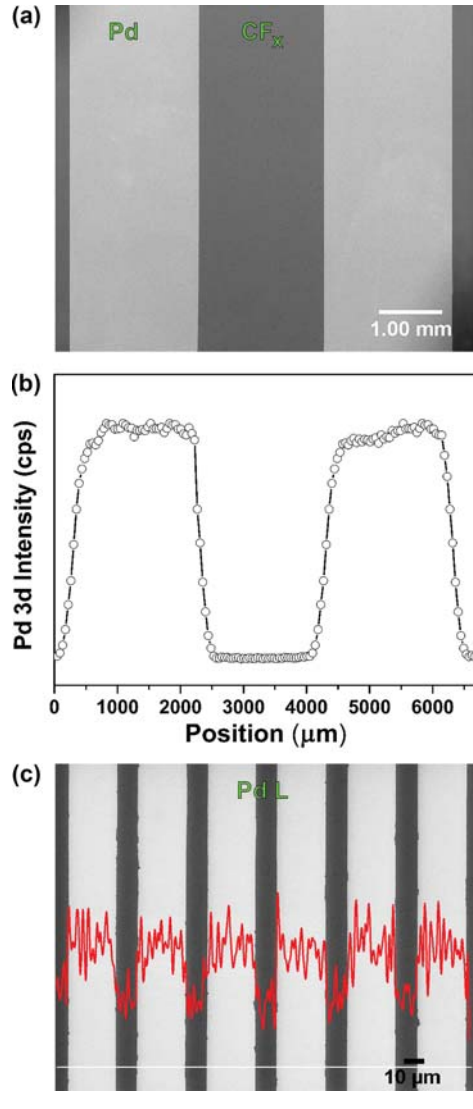
This is the author's peer reviewed, accepted manuscript. However, the online version of record will be different from this version once it has been copyedited and typeset.
PLEASE CITE THIS ARTICLE AS DOI: 10.1116/6.0000701



This is the author's peer reviewed, accepted manuscript. However, the online version of record will be different from this version once it has been copyedited and typeset.
PLEASE CITE THIS ARTICLE AS DOI: 10.1116/6.0000701



This is the author's peer reviewed, accepted manuscript. However, the online version of record will be different from this version once it has been copyedited and typeset.
PLEASE CITE THIS ARTICLE AS DOI: 10.1116/1.6.0000701



This is the author's peer reviewed, accepted manuscript. However, the online version of record will be different from this version once it has been copyedited and typeset.
PLEASE CITE THIS ARTICLE AS DOI: 10.1116/6.0000701

